Mechanics of Materials 159 (2021) 103900

Contents lists available at ScienceDirect

Mechanics of Materials

journal homepage: www.elsevier.com/locate/mechmat

Effect of plastic deformation on the nanomechanical properties of glassy polymers: An experimental study

Peyman Nikaeen [a], Aref Samadi-Dooki [b,*,1], George Z. Voyiadjis [b], Pengfei Zhang [a,c], William M. Chirdon [a], Ahmed Khattab [a]

[a] Laboratory of Composite Materials, Department of Mechanical Engineering, University of Louisiana at Lafayette, Lafayette, LA, 70504, USA
[b] Computational Solid Mechanics Laboratory (CSMLab), Department of Civil and Environmental Engineering, Louisiana State University, Baton Rouge, LA, 70803, USA
[c] School of Electromechanic Engineering, Qingdao University, Qingdao, 266071, China

ARTICLE INFO

Keywords:
Shear transformation zone
Nanomechanics
Polymeric glasses
Free volume

ABSTRACT

In this study, the effect of the macro-scale mechanical deformation on the nanostructure of glassy polymers is investigated by scrutinizing the alteration of their nanoscale mechanical response. Nanoindentation technique was used to measure the mechanical properties of the polycarbonate and poly(methyl methacrylate) specimens which were subjected to a prior plastic deformation in uniaxial tension. While the elastic part of the deformation induces reversible nanostructural reordering, it is the plastic part that brings about permanent/irreversible rearrangements. Hence, the measurements were only focused on the inelastically deformed and unloaded specimens. By incorporating the homogeneous flow theory and strain rate dependency of the plastic flow in nanoindentation, activation volume of the localized shear transformation zones that mediate the plasticity was calculated. The results show that the shear activation volume decreases with inelastic deformation. Considering the interrelation between the shear activation volume and the free volume content as the nanostructural defect in glassy polymers, this observation is well supported by the previously observed increase in defects upon plastic deformation for glassy polymers. Besides, the variation of hardness and modulus with plastic deformation history of the polymer is presented and discussed in this paper.

1. Introduction

Polymeric glasses (PGs) have become ubiquitously present in the daily lives in a wide range of applications, from eyeglass lenses to medical prostheses, composite panels in aircrafts to space structures, and electronic devices (Roth, 2017; Hiemenz and Lodge, 2007; Mittal, 2011; Zhao and Zikry, 2015). Thanks to their unique characteristics including a wide range of thermomechanical properties, they exhibit good processability that allows building complex shapes through traditional and modern manufacturing methods, e.g., injection molding and 3D printing (Roth, 2017; Hiemenz and Lodge, 2007). Nevertheless, any structural or nonstructural polymeric element requires to satisfy some load-bearing expectations; hence, it is of essential importance to understand and predict their mechanical properties at different length scales. Glassy polymers are generally categorized as visco-elasto-plastic materials, i.e., their small- and large-deformation mechanical behaviors are rate and time-dependent. Moreover, temperature and thermomechanical history of the PGs are known to affect their mechanical properties significantly (Argon, 2013). On the other hand, describing large deformation response of glassy polymers has always been a serious challenge in the field of material science and solid-state physics (Voyiadjis and Samadi-Dooki, 2016; Boyce et al., 1988). Unlike crystalline solids which have long-range structural coherence with dislocations as the mobile carriers of plasticity, amorphous polymers have virtually no significant order in their molecular structures resulting in a different mechanism of plastic deformation. In other words, due to the absence of regular lattices in glassy solids, variants of alternate mechanisms are believed to mediate plasticity in these materials (Argon, 2013).

Early efforts to understand the plasticity mechanisms of glassy polymers can be traced back to the work of Eyring who proposed molecular rearrangement during deformation (chain conformational transformations) as the main mechanism of the plastic flow (Eyring, 1936). Since then, researchers have built numerous large deformation

* Corresponding author.
E-mail address: rfdooki@gmail.com (A. Samadi-Dooki).
[1] Currently at DuPont Electronics and Industrial, Wilmington, DE 19803, USA.

https://doi.org/10.1016/j.mechmat.2021.103900
Received 2 December 2020; Received in revised form 29 March 2021; Accepted 2 May 2021
Available online 17 May 2021

models for polymers upon the macromolecular chain rearrangement (Argon, 1973, 2013; Boyce et al., 1988; Robertson, 1966; Arruda et al., 1995); including Boyce and coworkers (Boyce et al., 1988) who proposed chain entanglement opening as the post-yield softening, and chain alignment as the post-yield hardening mechanisms.

Although these models seemed to be appropriate for glasses with no long-range molecular order, by thermodynamic measurements of the plastically deformed PGs, Oleinik (Oleinik, 1991; Oleinik et al., 2007) showed that a considerable amount of energy is stored in the sample after unloading. While such a level of stored energy cannot be described in terms of conformational chain rearrangements, he suggested that it arises from non-vanishing elastic fields (after unloading) that form around permanently deformed plastic units. Oleinik's suggested mechanism was similar to the localized transformation theory, which had been proposed to mediate plastic deformation in metallic glasses (Spaepen, 1977; Argon, 1979). After years of development, it is now accepted among researchers that one common mechanism governs the plasticity of all disordered solids, whether polymeric, metallic, or covalent in nature. In this mechanism, nucleation of discrete irreversible rearrangements of atomic/molecular clusters upon yielding, which are called the shear transformation zones (STZs), yields the main rate-controlling event of the whole plastic deformation (Argon, 2013; Falk, 2007). These sites act as carriers of plasticity and have long-range elastic fields around them, similar to Eshelby's inclusion model (Eshelby, 1957). These elastic fields are the main sources of the energy excess which was observed in experimental studies of Oleinik (Oleinik, 1991; Oleinik et al., 2007) for plastically deformed PGs.

The shear transformation theory, which was originally proposed to explain the plasticity in metallic glasses by Spaepen (1977) and Argon (1979) and later re-formulated by Falk and coworkers (Falk, 2007), has been proven to be a well-founded method to describe the plastic deformation of PGs as well (Argon, 2013; Voyiadjis and Samadi-Dooki, 2016; Hasan et al., 1993). Computer simulations have shown that these zones are associated with regions of the enhanced structural disorder (Schuh and Lund, 2003) and nucleate in a cooperative manner, i.e., their transformation can induce the formation of new STZs. According to this theory, STZs are irreversible and thermally activated, and once formed, due to the absence of long-range structural coherence in PGs, they are not able to expand by translational movements of their boundaries (Argon, 2013). In other words, the plasticity of PGs mediated by shear transformations is nucleation controlled (Argon, 2013; Mott et al., 1993; Spathis and Kontou, 2001).

From the thermodynamics point of view, a polymeric glass is a nonequilibrium material formed because of packing frustration. As it is cooled to a solid from the fluid-like state, at a certain point, the system becomes non-ergodic due to insufficient thermal energy at the given time scale. The polymeric molecular chains are trapped in a nonequilibrium state associated with the condition they underwent at the point of vitrification (glass formation). At this state, a PG possesses a higher volume and configurational entropy compared to its equilibrium state due to the formation of excessive frozen-in free volume during vitrification (Roth, 2017). After they are formed, glasses start to move from a metastable state towards an equilibrium state through slow and gradually continual relaxation process which is called physical aging (Struik, 1977; Malekmotiei et al., 2017; Martinez-Vega et al., 2002). The study of free volume evolution upon thermal treatment has been carried out by many researchers to explore the correlation between the resulting nano and microstructural changes and the changes in mechanical properties of amorphous polymers (Hasan et al., 1993; Malekmotiei et al., 2017; Sandreczki et al., 1996; Tanio and Nakanishi, 2006; Cangialosi et al., 2003; Gunel and Basaran, 2011, 2013). In a recent study by Malekmotiei et al. (2017), the effect of annealing process on the microstructural and micromechanical properties of poly(methyl methacrylate) (PMMA) and polycarbonate (PC) was investigated using positron annihilation lifetime spectroscopy (PALS) and nanoindentation techniques. Based on that study, average free volume size (as the nanostructural state variable) changes in the opposite direction to the shear activation volume size (as the micromechanical state variable which is correlated with STZs). Malekmotiei et al. (2017) also demonstrated that annealing at temperatures close or above T_g of PC and PMMA is not beneficial for their mechanical strengthening since the increase of free volume content leads to facilitated flow of the material.

Nanostructural state and free volume content of the PGs are not solely functions of their thermal history but also affected by their prior exposure to mechanical deformations (Hasan et al., 1993; Hasan and Boyce, 1993; Oleinik et al., 2006; Lee and Ediger, 2010). In general, inelastic deformation changes the nanostructural state of the PGs, and accordingly, their micro- and macro-mechanical response to subsequent external loadings (Hasan et al., 1993). Accordingly, some studies have been focused on the effect of plastic deformation on the PGs' nanostructural state to investigate the nature of the disturbance mechanisms during plastic deformation to elucidate micromechanics of the deformations and visualize its different stages (Hasan et al., 1993; Hasan and Boyce, 1993; Oleinik et al., 2006; Lee and Ediger, 2010). Hasan et al. (1993) conducted PALS measurements on PMMA samples subjected to different thermal and inelastic compressive deformations and found that free volume content monotonically increases with inelastic strain until it reaches a steady state. In addition, they observed that the free volume content of annealed and quenched samples, although different at zero strain, eventually become equal after adequate inelastic deformation. Therefore, inelastic deformation is observed to erase the effect of prior thermal history and indeed increase free volume content with a corresponding drop in the yield stress after a certain point of plastic strain.

Based on the above-mentioned findings, the inelastic deformation and nanostructural state of PGs reciprocally affect each other. However, unlike the effect of physical aging, a proper interrelation between micro- and macro-scale evolutions upon inelastic deformations of PGs is seldom presented in the literature. Therefore, this study was aimed at utilizing the nanoindentation technique to evaluate the flow stress of PGs subjected to different prior inelastic deformations. Uniaxial tensile testing coupled with Digital Image Correlation (DIC) technique was used to precisely induce and monitor the plastic strain in the samples over the region intended for subsequent nanoindentation measurements. Using the homogeneous deformation theory for STZ mediated plasticity and strain sensitivity of the flow in glassy polymers, the nanomechanical properties of STZs were obtained employing nanoindentation results. In particular, the effect of inelastic straining on the shear activation volume of STZs is scrutinized, and its interrelation with free volume evolution due to plastic deformation is discussed.

2. Experimental procedure

2.1. Sample preparation

Commercially available amorphous poly(methyl methacrylate) (PMMA) and Lexan® polycarbonate (PC) sheets, with a thickness of 5 and 2.4 mm, respectively, were selected for this study. For the nanoindentation testing of the as-received materials, sheets were cut into small pieces of 150 × 150mm squares and then mounted on the aluminum stub using superglue. The surface of all samples was first thoroughly washed using isopropyl alcohol (IPA) and deionized water to remove any contamination. All samples were then stored in a desiccator for at least one week to remove any moisture from the washing process. The surface of samples made of both materials were optically smooth, hence, no polishing was required to prepare them for nanoindentation. The glass transition temperature (Tg) of the samples were measured using Perkin-Elmer 4000 differential scanning calorimeter (DSC). Purging gas used was compressed nitrogen with purging rate at 20 ml/min and standard aluminum pans were used to encapsulate the samples. The DSC tests were performed at a ramp rate of 10 °C/min from the ambient temperature up to 200 and 250 °C for PMMA and PC, respectively. The glass transition temperature was measured to be about

105 °C for PMMA and 148 °C for PC samples. Since the focus of this study was to investigate the effect of the prior plastic deformation on the nanomechanical properties of PGs, all tests, including tension and nanoindentation, were performed at room temperature (significantly below T_g).

To investigate the effect of the plastic deformation on the nanoindentation response of the polymers, dog-bone shape specimens were prepared according to ASTM D638-14 type 1 using a waterjet machine (Fig. 1(a)). The pre-test moisture removal process for the dog-bone samples was similar to that for the nanoindentation specimens.

2.2. Tensile tests with Digital Image Correlation strain measurement

Tensile test specimens were tested using an Instron 5982 Universal Testing Machine equipped with a DIC apparatus for accurate measurement of the strain contour (Fig. 1(c)). DIC is a non-contact optical measurement technique that uses a series of images of the surface of the object to calculate full-field surface deformation under load. It is based on examining the pixel density of the two subsets of images from the speckle patterned surface during deformation. Due to the transparent characteristic of the tested glassy polymers, one side of the specimens was sprayed with a black on white speckled pattern for imaging and data processing (Nath and Mokhtari, 2018). Special care was taken to apply a very thin layer of paint to minimize the impact of solvent on the mechanical properties of the polymer during the tensile test while preserving the quality of images for post-processing. Fig. 1(a)–(d) show the DIC tensile test experimental setup and a speckle patterned specimen surface before and after testing and analysis. Two LED light sources were placed leveled with the specimen to ensure that the speckled pattern on the gauge length area was identified by the two 12.0 Megapixel cameras. The servo-controlled load frame setup recorded the tensile load throughout the test. Load data acquisition from the tensile test machine and DIC image capturing were synchronized and the camera and image processing setup were calibrated before running the tests. The strain measurement noise level was found to be less than ±0.03% at no-load condition which is negligible in the current study. The isothermal uniaxial tensile tests were performed at room temperature and a constant engineering strain rate of 0.02% s^{-1}. The DIC data acquisition was continued for 2 min after the specimen failure to account for any strain recovery due to the viscoelastic nature of the samples. Therefore, a non-zero residual strain 2 min post-failure (unloading) was considered as an indicator of a plastic deformation in the specimen. The uniaxial tensile strain in the loading direction was averaged over the region of interest and reported for further analysis. Hereafter, the irreversible engineering plastic strain measured by the DIC method is denoted by ε_{irr}.

2.3. Nanoindentation

To investigate the correlation between nanostructural state and plasticity response of glassy polymers, depth-sensing indentation method was utilized in this study. Otherwise known as nanoindentation, this technique has recently become popular in the mechanical and microstructural characterization of polymers due to its repeatability and ease of use (Nikaeen et al., 2019; Vu et al., 2020; Voyiadjis et al., 2017; Zhang et al., 2018; Flores et al., 2009). A Nanoindenter G200 equipped with a three-sided pyramidal-shaped Berkovich tip was used to carry out the nanoindentation experiments at room temperature. Tip area calibration was performed prior to the main experiments to account for the tip imperfections and its deviation from an ideal geometry. Continuous stiffness measurement (CSM) technique was utilized to collect the mechanical properties throughout the whole indentation depth with a 2 nm amplitude and 45 Hz frequency oscillating sinusoidal load which was superimposed on the primary monotonically increasing load signal. To ensure the constant indentation strain rate, the loading segment was applied such that the loading rate divided by the load ratio ($\dot{P}/P$) was maintained at a constant value (see (Voyiadjis et al., 2019; Voyiadjis and Malekmotiei, 2016) for details). A hold segment was applied after loading to allow for the creep of the material, which is followed by the unloading at a constant rate. The output data of the nanoindentation experiment was analyzed according to the most common formalism developed by Oliver and Pharr (1992) to calculate the mechanical properties of the material. Accordingly, hardness H is calculated as:

$$H = \frac{P}{A_c} \tag{1}$$

where P is the applied indentation load and A_c is the projected contact area. The contact area is described according to Oliver and Pharr (1992) by a polynomial function of contact depth h_c as follows:

$$A_c = 24.56h_c^2 + C_1h_c^1 + C_2h_c^{\frac{1}{2}} + C_3h_c^{\frac{1}{4}} + C_4h_c^{\frac{1}{8}} + \ldots + C_8h_c^{\frac{1}{128}} \tag{2}$$

While the first term on the right-hand side of Eq. (2) represents the area function of a perfect Berkovich tip, other terms account for the

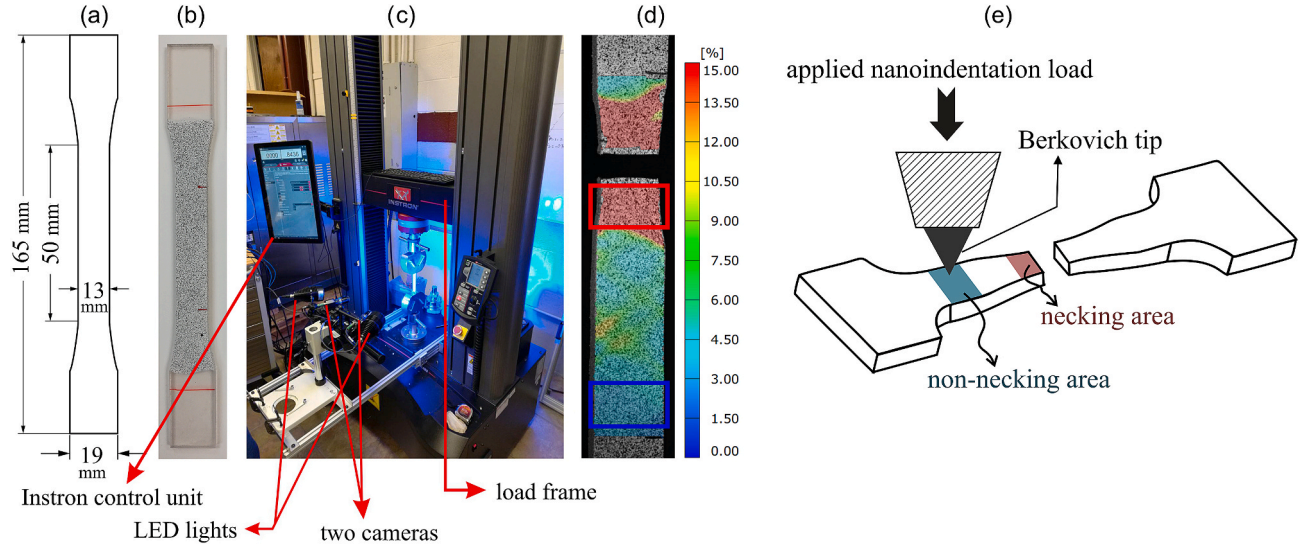

Fig. 1. a) geometry of the tensile test coupons according to ASTM D-638-14 type1, b) white and black speckled pattern for DIC measurements, c) universal tensile test machine equipped with DIC camera setup, d) strain contour of a representative PC specimen after failure, e) subsequent nanoindentation test on the plastically deformed samples.

deviation from an ideal shape. Accordingly, the constants C_i should be obtained for the diamond tip before running the tests on the samples through an empirical fitting process utilizing the results of indentations on fused silica.

The elastic modulus of the material is calculated from the reduced elastic modulus, E_r, as:

$$E = \left(1-\nu_s^2\right)\left[\frac{1}{E_r} - \frac{1-\nu_i^2}{E_i}\right]^{-1} \tag{3}$$

where E_i and ν_i are the Young's modulus and Poisson's ratio of the indenter, respectively, and ν_s is the Poisson's ratio of the tested specimen. While for a diamond tip, $\nu_i = 0.07$ and $E_i = 1141$ GPa, the Poisson's ratio of PC and PMMA are close to 0.38 and 0.37, respectively (Samadi-Dooki et al., 2016; Malekmotiei et al., 2015). The reduced elastic modulus which accounts for elastic deformation of both tip and the tested material is obtained as:

$$E_r = \frac{S}{2\lambda}\sqrt{\frac{\pi}{A_c}} \tag{4}$$

in which λ is a constant equal to 1.034 for a Berkovich tip, and S is the contact stiffness which for a CSM indentation is expressed as:

$$S = \left[\frac{1}{\frac{P_o}{h_{os}}\cos(\varphi) - (K_s - m\omega^2)} - \frac{1}{K_f}\right]^{-1} \tag{5}$$

where K_s and K_f represent the internal spring and the indenter frame stiffnesses, respectively, m is the indenter mass, and P_o and h_{os} are the amplitudes of the superimposed sinusoidal load and displacement, respectively. According to Eq. (5), the angular frequency of the load and displacement is equal to ω and the displacement lags the load by a phase shift of φ.

Since the rate sensitivity characteristic of the flow was used to calculate the nanomechanical and geometrical properties of the shear transformation units in this study, nanoindentation tests were performed at different indentation strain rates. The indentation strain rate $\dot{\varepsilon}_i$ is proportional to the loading rate divided by the load ratio ($\dot{P}/P$). This ratio can be satisfactorily maintained at a constant value during CSM nanoindentation (see (Voyiadjis et al., 2019; Voyiadjis and Malekmotiei, 2016) for details and discussion). In order to convert the nanoindentation strain rate to the shear strain rate, the following relation is used (Malekmotiei et al., 2015):

$$\dot{\gamma} = \frac{\sqrt{3}\,C}{\theta}\frac{\dot{P}}{P} \tag{6}$$

where the tip geometry dependent constant θ is equal to 2 for a Berkovich tip, and C is a constant equal to 0.09 (Schuh and Nieh, 2003; Poisl et al., 1995).

To investigate the mechanical response of the PMMA and PC samples, nanoindentation tests at eight $\dot{P}/P$ values ranging from 0.002 to 0.15s^{-1} were conducted at room temperature. At each strain rate, 25 tests were performed with a maximum indentation depth of 10 μm and a spacing of 200 μm to avoid the effect of interactions of plastic deformations of the adjacent indents.

3. Theory: homogeneous flow of glassy polymers

The plastic deformation of a glassy solid might follow one of the two basic modes of flow (Spaepen, 1977): (I) a homogeneous flow associated with the cooperative contribution of the localized rearranged atomic (in metallic glasses) or molecular (in polymeric glasses) clusters to the total plastic strain; the units that carry plastic strains are called shear transformation zones (STZs). (II) an inhomogeneous flow where the strain is localized by coalescence of STZs in a few very thin shear bands. Homogeneous and inhomogeneous flow in PGs can be differentiated by their distinct characteristics; homogeneous flow is shown to be sensitive to strain rate in a sense that with increasing the rate the material exhibits a higher flow stress. In contrary, the inhomogeneous flow is strain rate insensitive (Spaepen, 1977). Moreover, inhomogeneous flow during nanoindentation of polymeric glasses has been shown to be manifested by multiple pop-in events in the load-displacement curve as opposed to the homogeneous flow where the curve is virtually smooth (Zhang et al., 2005; Golovin et al., 2001). In order to investigate the nature of flow in PMMA and PC samples in this study, load-displacement curves of the nanoindentation tests performed on both undeformed and deformed (in tension) samples at different strain rates were analyzed (Fig. 2) and no pop-in event was observed. Moreover, Figs. 3 and 4 illustrate the dependence of hardness of both materials on the strain rate. Considering the direct relation between hardness H and yield stress σ_y with a proportionality factor of κ (Tabor's relation $H = \kappa\sigma_y$), this rate sensitivity serves as another indication of the homogeneous nature of the flow of the tested polymers. This observation is in a good agreement with the study by Casas et al. (2008).

Thermally activated homogeneous flow in amorphous polymers can be described by the flow model developed by Spaepen (1977) and Argon (1979), which was originally developed for metallic glasses. According to the STZ mediated homogeneous flow, the kinetic relation between the applied shear stress τ and the shear strain rate $\dot{\gamma}$ can be expressed by an Arrhenius relation as follows:

$$\dot{\gamma} = \dot{\gamma}_0 \exp\left(-\frac{\Delta G}{k_B T}\right)\sinh\left(\frac{\gamma^T \Omega \tau}{2k_B T}\right) \tag{7}$$

in which k_B is the Boltzmann constant, T is the absolute temperature, and $\dot{\gamma}_0$ is the pre-exponential factor proportional to the attempt frequency. The other three variables are related to the STZs; Ω is the volume of an STZ, γ^T is the transformation shear strain it contains, and ΔG is its nucleation free energy. For conventional PGs at temperatures below their glass transition, one can assume $\gamma^T\Omega\tau \gg 2k_BT$; this results in a rearranged form of Eq. (7) as $\ln(\dot{\gamma}) = \frac{\gamma^T\Omega}{2k_BT}\tau + C_1$ with $C_1 = \ln\left(\frac{\dot{\gamma}_0}{2}\right) - \frac{\Delta G}{k_BT}$ representing a stress-independent parameter. At a given temperature, this rearranged expression represents a linear relation between the natural logarithm of shear strain rate $\ln(\dot{\gamma})$ and shear stress τ with a slope of $\frac{\gamma^T\Omega}{2k_BT}$. It is known that under monotonic loading condition, the shear flow stress is nearly half of the maximum plane stress at yield. Hence, by considering the previously explained Tabor's relation and a κ factor value of 3.3 for glassy polymers (Prasad et al., 2009), one can readily convert the hardness obtained by nanoindentation to shear flow stress by dividing it by 6.6. Accordingly, by performing nanoindentation tests at different strain rates and recording hardness values, one can use the above linear correlation to calculate $\gamma^T\Omega$. The shear activation volume (V^*) of the plasticity units can then be calculated by Eq. (8) as follows:

$$V^* = (1+\beta\alpha)\gamma^T\Omega \tag{8}$$

where β is the dilatancy parameter obtained from the pressure sensitivity of the yielding, and α is a constant related to the loading condition. In equation (8), the shear activation volume is calculated by modifying the STZ volume (Ω) with consideration of the dilatation effect.

4. Results and discussion

The results of the tensile tests with DIC on PC and PMMA are shown in Figs. 5 and 6, respectively. In Fig. 5 the evolution of engineering stress versus engineering strain in the necking region, non-necking area, and the whole gauge length are demonstrated for PC. Two zones of interest for nanoindentation measurements in the transverse direction were chosen in areas with homogeneous distribution of strains and subjected to different inelastic straining: one necking area which ended up

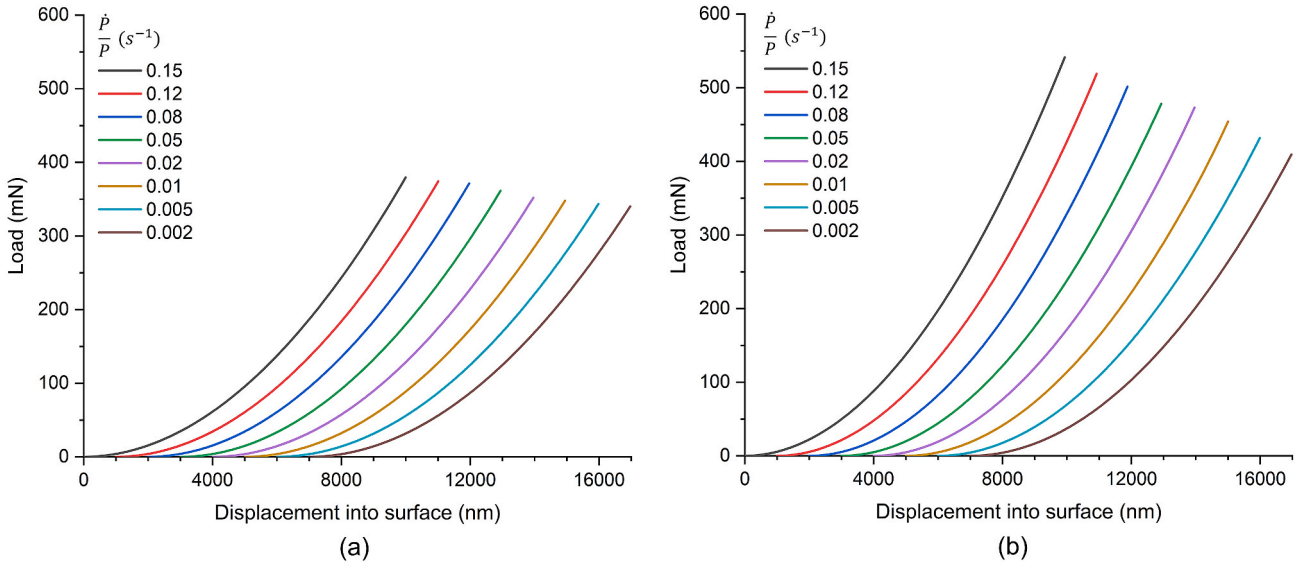

Fig. 2. Load-displacement into surface curves for deformed (a) PC and (b) PMMA samples at different strain rates (legend numbers indicate $\dot{P}/\ P\ (s^{-1})$ values). Origin offset of 1 μm is applied for all curves except for the ones associated with $\dot{P}/P$ of 0.15 s^{-1}. Similar smooth curves are observed for undeformed samples, which are not shown herein for brevity. No pop-in event is observed in any of the tests.

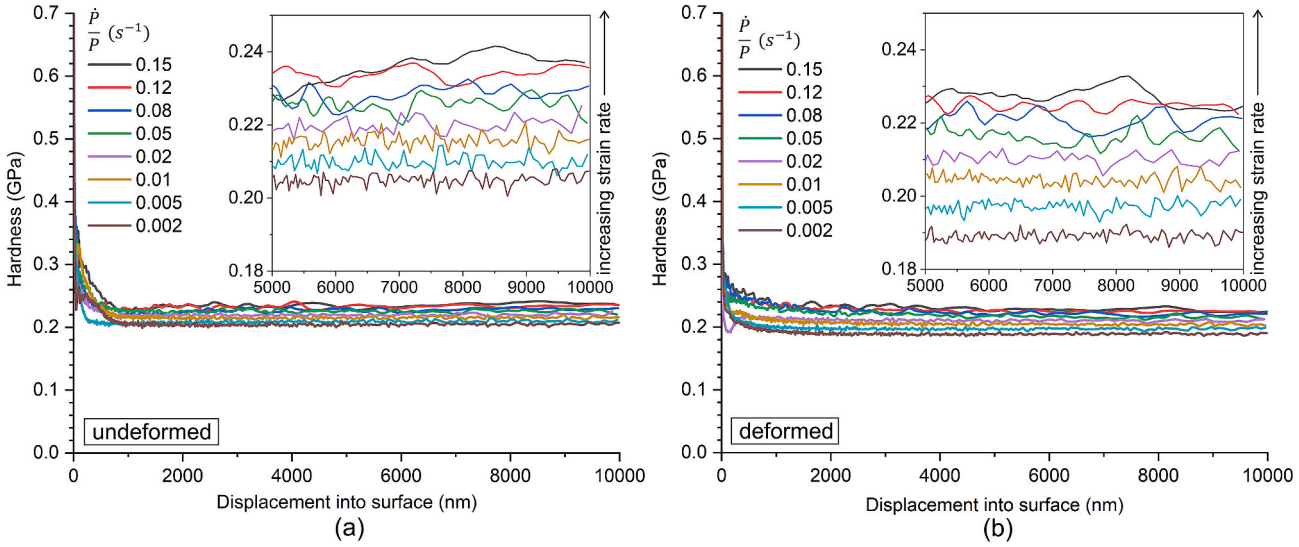

Fig. 3. Variation of hardness with the indentation depth for (a) undeformed and (b) deformed (40.5% ε_{irr}) PC samples at different $\dot{P}/P$ values (as indicated in the legend).

maintaining a steady value of 40.5% irreversible strain (shown as a red rectangle in Fig. 5) and one non-necking area with 2.6% irreversible strain 2 min after failure (shown as a blue rectangle in Fig. 5). Strain gradient with the localized concentration on the necking area for PC samples indicates the sample underwent ductile stretching and necking before failure. In contrast, it is seen in Fig. 6 that PMMA experienced a brittle fracture with a maximum engineering strain of around 3% with no signs of necking. After fracture and releasing the elastic strain, the plastic strain reduced to around 0.4%, and eventually after 2 min of strain recovery it reached a steady irreversible value of 0.2%. The red rectangle in Fig. 6 designates the chosen area for the nanoindentation measurements for the deformed PMMA sample.

The nanomechanical response of the plastically deformed samples was measured using nanoindentation. Continuous Stiffness Measurement method was used to record the properties throughout the whole indentation depth. Figs. 3 and 4 show the variation of hardness, and Figs. 7 and 8 show the variation of elastic modulus of all samples with indentation depth up to 10 μm. Each curve in these figures represents the average response of 25 indents at that rate. It can be observed that the nanoindentation results have apparent variation at very shallow depths due to indentation size effects (ISE) (Voyiadjis et al., 2018; Pharr et al., 2010). However, recorded values reach a plateau after a certain depth (around 600 nm) and can be considered as the bulk properties of the samples. Accordingly, at each rate, the bulk elastic modulus and hardness were obtained by averaging the values between 5 and 10 μm for all 25 indents at that rate. Also, the maximum coefficient of variation (COV) of the nanoindentation results for each rate for the undeformed and deformed PMMA samples was calculated at 0.4% and 0.7%, respectively, and that for undeformed and deformed PC samples were calculated at 1.5% and 0.7%, respectively. Low COV of the obtained nanoindentation results verifies the validity, consistency, and repeatability of the whole experimental procedure to extract the mechanical properties.

It is noticeable from Figs. 7 and 8 that the strain rate does not seem to

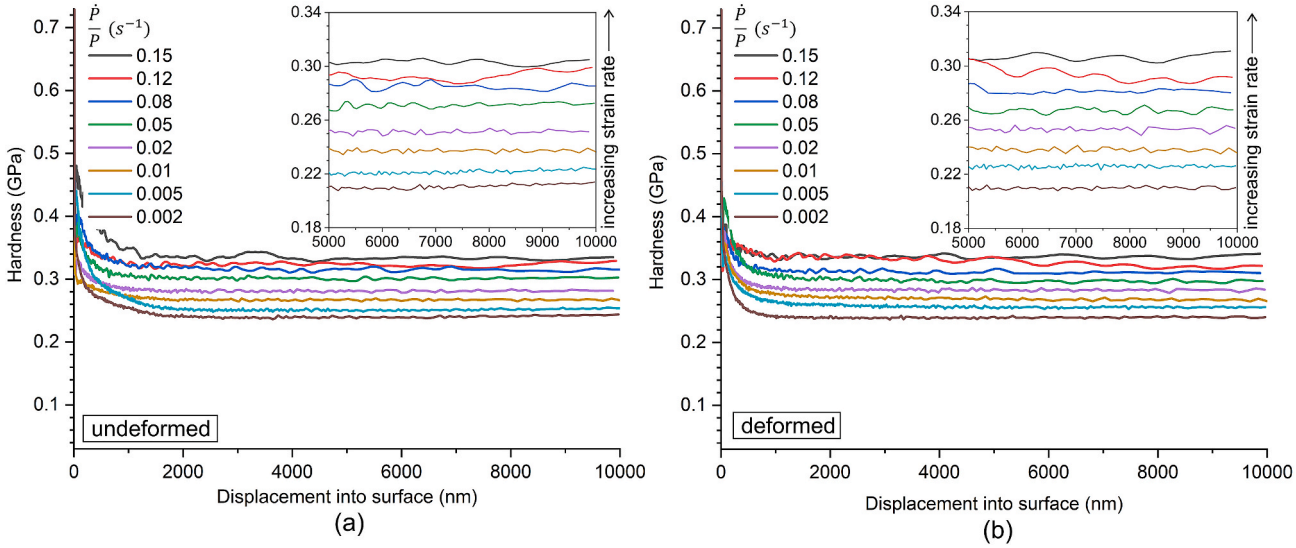

Fig. 4. Variation of hardness with the indentation depth for (a) undeformed and (b) deformed (0.2% ε_{irr}) PMMA samples at different $\dot{P}/P$ values (as indicated in the legend).

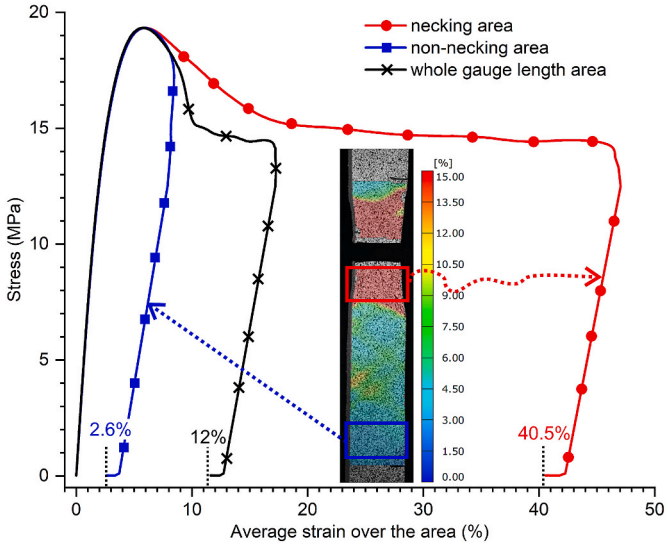

Fig. 5. Inelastic deformation of PC samples monitored by DIC during tension with 40.5% and 2.6% irreversible strain 2 min post-failure for necking and non-necking regions, respectively. Each strain-stress curve corresponds to the areas shown in colored rectangular box, and the black stress-strain curve corresponds to the whole gauge length area.

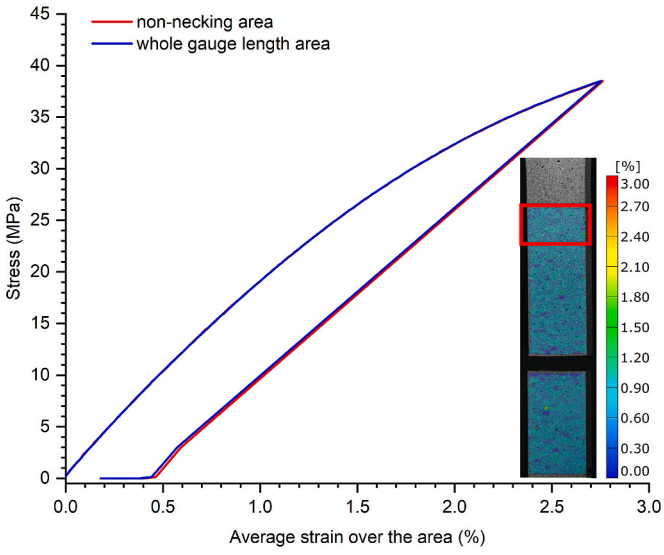

Fig. 6. Inelastic deformation of PMMA samples monitored by DIC during tension with 0.2% irreversible strain 2 min post-failure. The distribution of irreversible plastic strain is consistent throughout the whole gauge length due to the brittle fracture.

alter the elastic modulus of either of the polymers to the same extent that it affects the hardness (flow stress); this observation is consistent with the fact that the elastic modulus is controlled by intermolecular van der Waals interactions in glassy polymers which are less sensitive to strain rate (Argon, 2013; Perez, 1998). On the other hand, the calculated hardness values exhibit a significant rate dependency as shown in Figs. 3 and 4 where a higher strain rate results in a higher recorded hardness value. The strain rate sensitivity character of the flow and the Arrhenius relation of Eq. (7) are employed to calculate the geometrical properties of the plasticity units in the homogeneous STZ mediated flow of the glassy polymers. In particular, the shear activation volume pertaining to the nanostructural state of the glasses before and after plastic deformation in tension is calculated using Eq. (8) and incorporating the slope of the variation of the shear flow stress versus the logarithm of shear strain rate curves (see Figs. 9 and 10 for PC and PMMA samples, respectively). Using α and β values of 0.65 and 0.27 for PC (Rittel and Dorogoy, 2008) and 0.65 and 0.204 for PMMA (Ward, 1971), respectively, shear activation volumes were calculated as shown in Table 1. The calculated V^* values for undeformed samples closely match the previously reported values based on experiments (Malekmotiei et al., 2017) and atomistic simulations (Argon, 2013). The current results, however, reveal that a history of plastic deformation decreases the shear activation volume for both glassy polymers.

Fig. 9 indicates the flow stress values of undeformed and deformed PC samples are significantly different such that with increasing the accumulated plastic strain in tension, the flow stress in the transverse direction decreases up to 10% (also see the insets in Fig. 3). Considering the dramatic post-yield softening of this material (see Fig. 5) and the fact that any reloading after unloading follows the same path as the unloading segment, this observation may suggest an isotropic plastic softening (contrary to an isotropic hardening) in this material; this

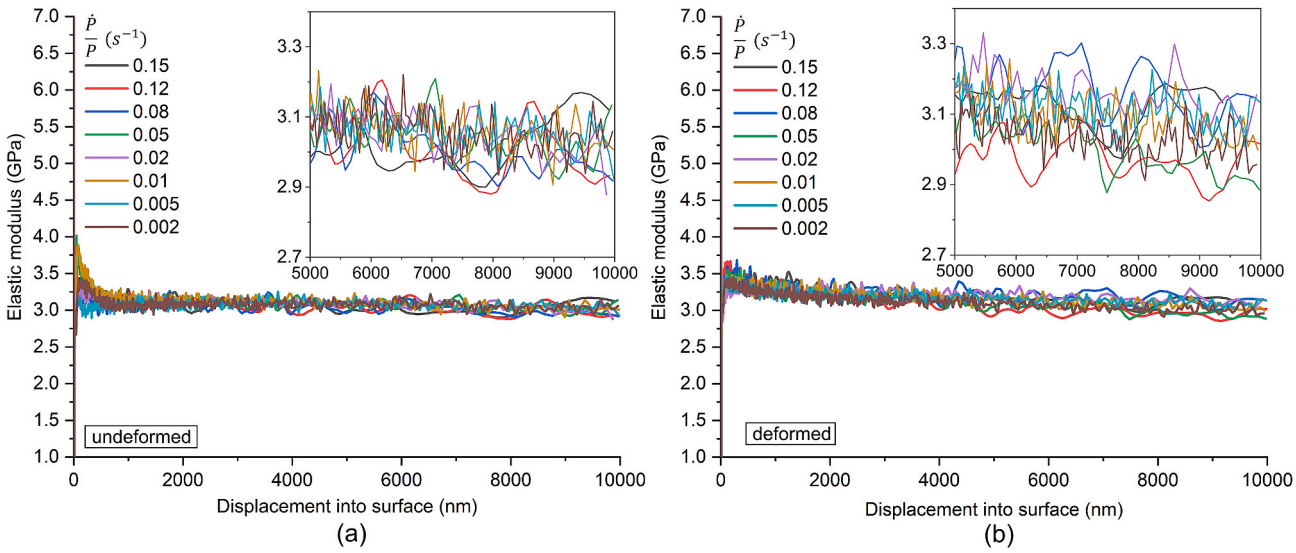

Fig. 7. Variation of elastic modulus *vs* the indentation depth for (a) undeformed and (b) deformed (40.5% ε_{irr}) PC samples at different $\dot{P}/P$ values (as indicated in the legend).

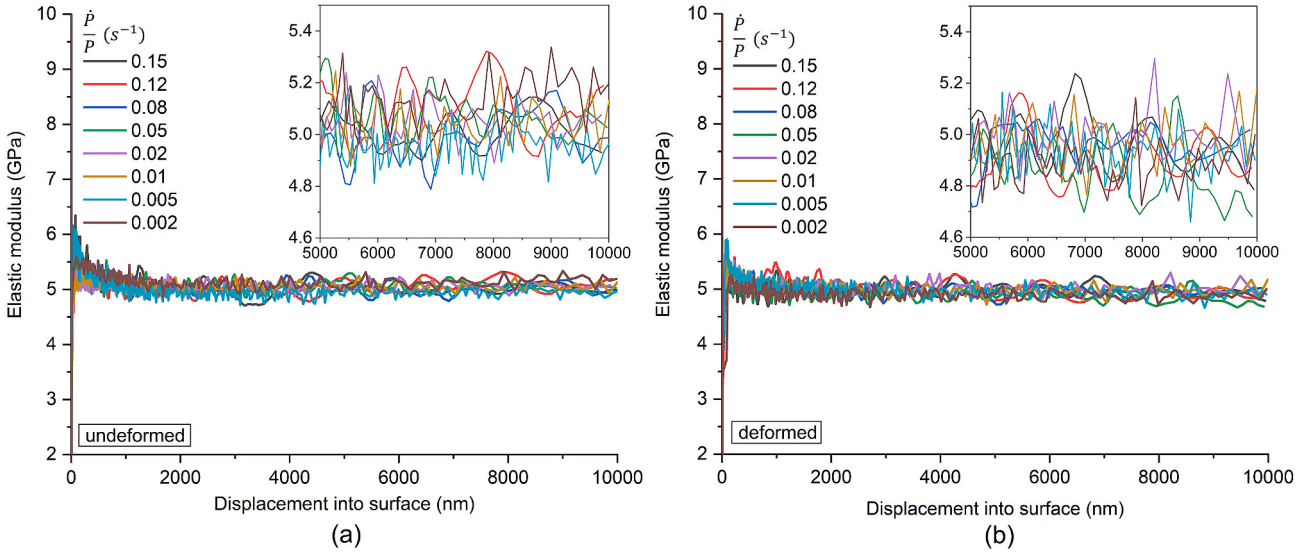

Fig. 8. Variation of elastic modulus *vs* the indentation depth for (a) undeformed and (b) deformed (0.2% ε_{irr}) PMMA samples at different $\dot{P}/P$ values (as indicated in the legend).

means a contraction of the yield surface as opposed to its expansion in isotropic hardening. Physically, the reduction of resistance to flow could be due to accumulated damage in the specimen at high strain levels; such damage mechanisms can emerge as voids and crazes which are usually detectable with optomechanical measurements (e.g., alteration of the refractive index (Kambour, 1964)) considering their size scales. Another reason might be the effect of the post-yield stretching on the chain alignment in the loading direction, which results in reduced flow resistance in the transverse direction. Also, the increased free volume ratio due to the plastic deformation (Hasan et al., 1993) can contribute to the reduction of the resistance of the material to subsequent plastic deformations. The latter mechanism will be further discussed in the following paragraph. As demonstrated in Fig. 10, the variation of flow stress for a plastically deformed PMMA sample does not show a significant difference with the intact one. This observation might be due to the brittle nature of the failure with negligible irreversible strains for PMMA. Nevertheless, the slope of the variation of the shear flow stress with the logarithm of the shear strain rate increases with even a small plastic deformation for this material. Another feature of the response of PMMA samples to variation of the strain rate is the double-linear variation of the shear flow stress versus the logarithm of the shear strain rate separating at shear strain rates of around 0.005 s^{-1}. This behavior which was previously reported in Malekmotiei et al. (2015), is associated with the activation of the so-called β-transition mechanism (Mulliken and Boyce, 2006; Roetling, 1965; Bauwens-Crowet, 1973). Restriction of the ester side group rotations at high strain rates, along with the intermolecular and local backbone motion restrictions are deemed to be the reasons for this transition in PMMA. Accordingly, only the α-regime (below the transition point) has relevant implications to be used for measuring shear activation volume in PMMA (Malekmotiei et al., 2015). Analogous to PC samples, a reduction of shear activation volume for PMMA samples has been observed in α-regime, where it decreased from 2.602 nm^3 for the undeformed state to 2.520 nm^3 after 0.2% irreversible strain. However, this reduction is not well pronounced as PC since the material has undergone relatively small plastic deformation before fracture at room temperature.

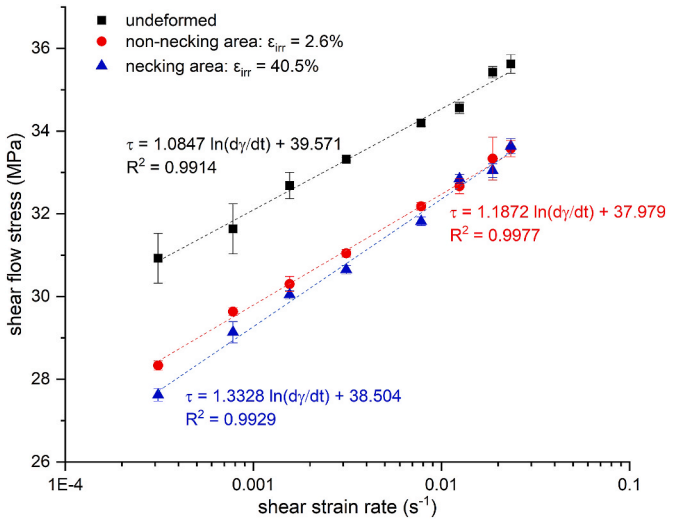

Fig. 9. Variation of shear flow stress with the shear strain rate for PC samples subjected to 0%, 2.6%, and 40.5% irreversible strain in tension. The dashed lines represent the logarithmic interpolation with the equation and R^2 value shown in the figure.

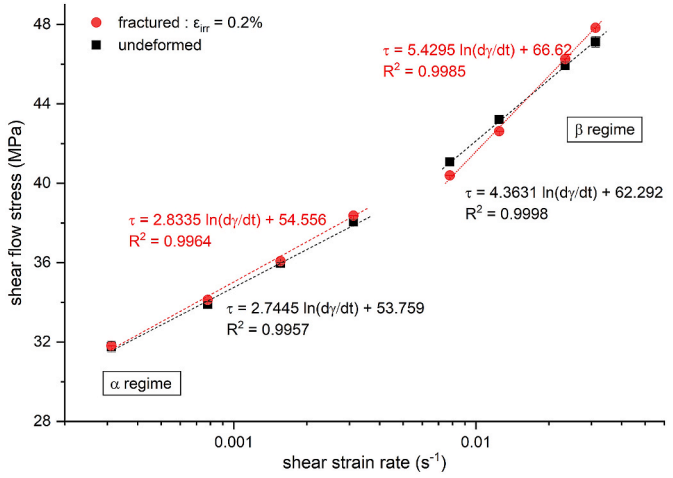

Fig. 10. Variation of shear flow stress with the shear strain rate for PMMA samples subjected to 0% and 0.2% irreversible strain in tension. The dashed lines represent the logarithmic interpolation with the equation and R^2 value shown in the figure.

Table 1
Shear activation volume (V^*) values calculated for PC and PMMA samples subjected to plastic deformation at room temperature.

V^* (PC)			V^* (PMMA)	
Undeformed	2.6% ε_{irr}	40.5% ε_{irr}	undeformed	0.2% ε_{irr}
6.258 NM^3	5.718 nm^3	5.093 nm^3	2.602 nm^3	2.520 nm^3

It is evident from the current experimental results that shear activation volume changes upon plastic deformation, indicating a change in the nanostructural sate of the polymer. For PC, the undeformed sample had a V^* of 6.258 nm^3, which was compacted to 5.718 nm^3 and 5.093 nm^3 after being subjected to 2.6% and 40.5% irreversible plastic strain, respectively. As originally described in the theory of shear transformation mediated plasticity by Argon (1979), the plastic units are deemed to nucleate in the proximity of the free volume cavities in glasses. Since the size of free volume holes is an order of magnitude smaller than V^* in PGs, they do not provide space for the required shear straining in STZs, whereas, by creating "weak spots," they act as fertile sites to initiate the shear transformations (Argon, 2013). Due to the importance of the interrelation between free volume content and micromechanics of flow, several studies have focused on free volume evolution upon plastic flow in glassy solids. According to Hasan et al. (Hasan and Boyce, 1993), inelastic deformation in PMMA increases the average size of the free volume sites as measured by PALS until it attains a steady value (which occurs around 30% compressive strain). Moreover, it was previously observed that the shear activation volume varies in the opposite direction of the free volume average size, i.e., the increased free volume size results in a decrease in the shear activation volume (Malekmotiei et al., 2017). Collectively, the decreased shear activation volume due to the increased accumulated plastic strain, as observed in this study, confirms the role of large deformation on the evolution of the free volume average size without directly measuring it.

In addition, it is well known that the increase of free volume average size (rejuvenation process) facilitates the flow mechanism in polymeric glasses by increasing the fertile sites for nucleation of STZs, and accordingly, an apparent reduction in yield stress and hardness values. One of the limitations of the current work is lack of direct measurement of the free volume content of the tested polymers. Nevertheless, strain field measured by the DIC technique was used to calculate the change of the volume with the uniaxial tension as shown in Fig. 11. The volume of both samples increased with increasing the uniaxial strain. For PC, the non-necking region experienced less than 1% volume increase for the axial strains up to 7%. For the necking region, the volume increased up to 6% uniaxial strain (which corresponds to the local maximum stress). Subsequently, the volume started to decrease slightly until the axial strain reached 15%. This stage corresponds to the reduction in the engineering stress. For uniaxial strains beyond 15%, the volume continued to increase monotonically and reached a 5% volume increase for a 45% uniaxial strain. For PMMA, the volume increased monotonically with the uniaxial strain up to the failure point. It should be noted that the change of the volume was calculated using the stretch values rather than the engineering strain (for detailed discussion on the relation between volume change and strain measures see (Voyiadjis and Samadi-Dooki, 2018)). The volume change calculated based on strain field measured by DIC might not exactly match the free volume change but is consistent with the expected trend of volume change.

From the experimental results provided in here and previous studies (Hasan et al., 1993; Malekmotiei et al., 2017), it can be concluded that inelastic deformation has a rejuvenation effect on glassy polymers by increasing the free volume content and erasing the effect of the thermal history. Therefore, annealing (as a physical aging process) and inelastic deformation are deemed to act oppositely in changing the nano- and microstructural state of PGs and their subsequent mechanical properties. This observation agrees with findings of a recent study by Malekmotiei et al. (2017) on PC and PMMA samples where it was found that shear activation volume and free volume content change in opposite directions upon annealing.

Lastly, it is important to note that the elastic modulus of both polymers did not seem to vary in a meaningful manner with the history of plastic deformation (see Figs. 7 and 8). This observation is consistent with the previous findings of the minimal effect of the thermal history on the elastic modulus of glassy polymers (Malekmotiei et al., 2015) and considering the fact that the plastic deformation has a similar effect on the nanostructure of polymer to the rejuvenation due to some thermal treatments such as quenching.

5. Conclusion

The fundamental core of the STZ mediated plastic flow mechanism in PGs is the nucleation of shear transformation units under external loading. However, there are yet many unknown aspects of the mechanism of such localized deformations to bring about the large-scale permanent plastic strain upon large deformations. This study sheds light on

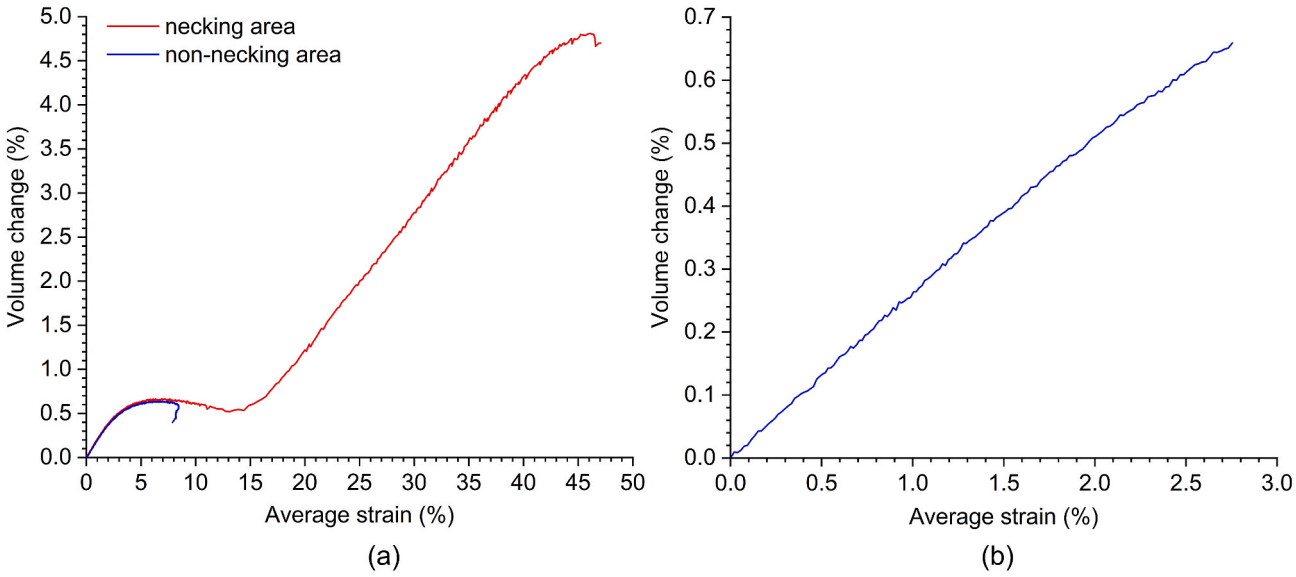

Fig. 11. Change of the volume *vs* applied uniaxial strain for (a) PC and (b) PMMA.

some aspects of the nanostructural state of the material in the shear transformation sites. Plastic deformation was selected as a mechanism to change the nanostructural state of the PC and PMMA, as two widely used glassy polymers, and the effect of such alterations on the characteristics of their flow units was investigated. For PC, it was observed that a history of in-plane plastic deformation results in lower resistance to additional plastic deformation in the transverse direction. The dramatic post-yield softening of this material may suggest an isotropic plastic softening with contraction of the yield surface. Such a conclusion cannot be made for PMMA due to a minimal plastic deformation before its failure. Moreover, it was observed that a history of plastic deformation results in the reduction of shear activation volume of the STZs for both polymers. Considering the interrelation between the shear activation volume and the free volume content of the polymers, this study suggests an alternate method for monitoring the damage accumulation in PGs (an increase of free volume content) without directly measuring it. Hence, nano-indentation can serve as a powerful tool for nondestructive health monitoring of load-bearing elements in NEMS, MEMS, small scale mechanical actuators, and the like.

Author statement

Peyman Nikaeen: Writing - original draft, Test execution, Data curation, Formal analysis, Investigation, Visualization. Aref Samadi-Dooki: Conceptualization, Methodology, Formal analysis, Writing - original draft, Writing - review & editing, Validation, Supervision. George Voyiadjis: Investigation, Writing - review & editing. Pengfei Zhang: Investigation, Writing - review & editing. William Chirdon: Investigation, Writing - review & editing. Ahmed Khattab: Investigation, Writing - review & editing, Funding acquisition, Supervision.

Declaration of competing interest

The authors declare that they have no known competing financial interests or personal relationships that could have appeared to influence the work reported in this paper.

Acknowledgments

The authors thank Drs. Mehdi Mokhtari and Prathmesh Naik Parrikar of the Department of Petroleum Engineering at ULL for their collaboration in performing DIC tensile tests. Peyman Nikaeen acknowledges partial financial support provided by the US National Science Foundation under grant number OIA-1946231 and the Louisiana Board of Regents for the Louisiana Materials Design Alliance (LAMDA).

References

Argon, A.S., 1973. A theory for the low-temperature plastic deformation of glassy polymers. Phil. Mag. 28 (4), 839–865.
Argon, A.S., 1979. Plastic deformation in metallic glasses. Acta Metall. 27 (1), 47–58.
Argon, A.S., 2013. The Physics of Deformation and Fracture of Polymers. Cambridge University Press, Cambridge.
Arruda, E.M., Boyce, M.C., Jayachandran, R., 1995. Effects of strain rate, temperature and thermomechanical coupling on the finite strain deformation of glassy polymers. Mech. Mater. 19 (2–3), 193–212.
Bauwens-Crowet, C., 1973. The compression yield behaviour of polymethyl methacrylate over a wide range of temperatures and strain-rates. J. Mater. Sci. 8 (7), 968–979.
Boyce, M.C., Parks, D.M., Argon, A.S., 1988. Large inelastic deformation of glassy polymers. part I: rate dependent constitutive model. Mech. Mater. 7 (1), 15–33.
Cangialosi, D., Schut, H., van Veen, A., Picken, S.J., 2003. Positron annihilation lifetime spectroscopy for measuring free volume during physical aging of polycarbonate. Macromolecules 36 (1), 142–147.
Casas, F., Alba-Simionesco, C., Montes, H., Lequeux, F., 2008. Length-scale of glassy polymer plastic flow: a neutron scattering study. Macromolecules 41 (3), 860–865.
Eshelby, J.D., 1957. The determination of the elastic field of an ellipsoidal inclusion, and related problems. Proc. Roy. Soc. Lond. A 241 (1226), 376–396.
Eyring, H., 1936. Viscosity, plasticity, and diffusion as examples of absolute reaction rates. J. Chem. Phys. 4 (4), 283–291.
Falk, M.L., 2007. Materials science. The flow of glass. Science 318 (5858), 1880–1881.
Flores, A., Ania, F., Baltá-Calleja, F.J., 2009. From the glassy state to ordered polymer structures: a microhardness study. Polymer 50 (3), 729–746.
Golovin, Y.I., Ivolgin, V.I., Khonik, V.A., Kitagawa, K., Tyurin, A.I., 2001. Serrated plastic flow during nanoindentation of a bulk metallic glass. Scripta Mater. 45 (8), 947–952.
Gunel, E.M., Basaran, C., 2011. Damage characterization in non-isothermal stretching of acrylics. Part I: Theory. Mech. Mater. 43 (12), 979–991.
Gunel, E., Basaran, C., 2013. Influence of filler content and interphase properties on large deformation micromechanics of particle filled acrylics. Mech. Mater. 57, 134–146.
Hasan, O.A., Boyce, M.C., 1993. Energy storage during inelastic deformation of glassy polymers. Polymer 34 (24), 5085–5092.
Hasan, O.A., Boyce, M.C., Li, X.S., Berko, S., 1993. An investigation of the yield and postyield behavior and corresponding structure of poly(methyl methacrylate). J. Polym. Sci. B Polym. Phys. 31 (2), 185–197.
Hiemenz, P.C., Lodge, T., 2007. Polymer Chemistry. CRC Press, Boca Raton, Florida.
Kambour, R.P., 1964. Refractive indices and compositions of crazes in several glassy polymers. J. Polym. Sci. A Gen. Pap. 2 (9), 4159–4163.
Lee, H.-N., Ediger, M.D., 2010. Mechanical rejuvenation in poly(methyl methacrylate) glasses? Molecular mobility after deformation. Macromolecules 43 (13), 5863–5873.
Malekmotiei, L., Samadi-Dooki, A., Voyiadjis, G.Z., 2015. Nanoindentation study of yielding and plasticity of poly(methyl methacrylate). Macromolecules 48 (15), 5348–5357.
Malekmotiei, L., Voyiadjis, G.Z., Samadi-Dooki, A., Lu, F., Zhou, J., 2017. Effect of annealing temperature on interrelation between the microstructural evolution and plastic deformation in polymers. J. Polym. Sci. B Polym. Phys. 55 (17), 1286–1297.
Martinez-Vega, J.J., Trumel, H., Gacougnolle, J.L., 2002. Plastic deformation and physical ageing in PMMA. Polymer 43 (18), 4979–4987.

Mittal, V., 2011. High Performance Polymers and Engineering Plastics. John Wiley & Sons, Inc, Hoboken, NJ, USA.
Mott, P.H., Argon, A.S., Suter, U.W., 1993. Atomistic modelling of plastic deformation of glassy polymers. Philos. Mag. A 67 (4), 931–978.
Mulliken, A.D., Boyce, M.C., 2006. Mechanics of the rate-dependent elastic–plastic deformation of glassy polymers from low to high strain rates. Int. J. Solid Struct. 43 (5), 1331–1356.
Nath, F., Mokhtari, M., 2018. Optical visualization of strain development and fracture propagation in laminated rocks. J. Petrol. Sci. Eng. 167, 354–365.
Nikaeen, P., Depan, D., Khattab, A., 2019. Surface mechanical characterization of carbon nanofiber reinforced low-density polyethylene by nanoindentation and comparison with bulk properties. Nanomaterials 9 (10).
Oleinik, E.F., Rudnev, S.N., Salamatina, O.B., Shenogin, S.V., Kotelyanskii, M.I., Paramzina, T.V., et al., 2006. Energy storage in cold non-elastic deformation of glassy polymers. E-Polymers 6 (1).
Oleinik, E., 1991. Distortional plasticity of organic glassy polymers. In: Baer, E., Moet, A. (Eds.), High Performance Polymers. Hanser, New York, pp. 79–102.
Oleinik, E.F., Rudnev, S.N., Salamatina, O.B., 2007. Evolution in concepts concerning the mechanism of plasticity in solid polymers after the 1950s. Polym. Sci. 49 (12), 1302–1327.
Oliver, W.C., Pharr, G.M., 1992. An improved technique for determining hardness and elastic modulus using load and displacement sensing indentation experiments. J. Mater. Res. 7 (6), 1564–1583.
Perez, J., 1998. Physics and Mechanics of Amorphous Polymers. Balkema.
Pharr, G.M., Herbert, E.G., Gao, Y., 2010. The indentation size effect: a critical examination of experimental observations and mechanistic interpretations. Annu. Rev. Mater. Res. 40 (1), 271–292.
Poisl, W.H., Oliver, W.C., Fabes, B.D., 1995. The relationship between indentation and uniaxial creep in amorphous selenium. J. Mater. Res. 10 (8), 2024–2032.
Prasad, K.E., Keryvin, V., Ramamurty, U., 2009. Pressure sensitive flow and constraint factor in amorphous materials below glass transition. J. Mater. Res. 24 (3), 890–897.
Rittel, D., Dorogoy, A., 2008. A methodology to assess the rate and pressure sensitivity of polymers over a wide range of strain rates. J. Mech. Phys. Solid. 56 (11), 3191–3205.
Robertson, R.E., 1966. Theory for the plasticity of glassy polymers. J. Chem. Phys. 44 (10), 3950–3956.
Roetling, J.A., 1965. Yield stress behaviour of polymethylmethacrylate. Polymer 6 (6), 311–317.
Roth, C.B., 2017. Polymer Glasses. CRC Press, Boca Raton.
Samadi-Dooki, A., Malekmotiei, L., Voyiadjis, G.Z., 2016. Characterizing shear transformation zones in polycarbonate using nanoindentation. Polymer 82, 238–245.
Sandreczki, T.C., Hong, X., Jean, Y.C., 1996. Sub-glass-transition-temperature annealing of polycarbonate studied by positron annihilation spectroscopy. Macromolecules 29 (11), 4015–4018.
Schuh, C.A., Lund, A.C., 2003. Atomistic basis for the plastic yield criterion of metallic glass. Nat. Mater. 2 (7), 449–452.
Schuh, C.A., Nieh, T.G., 2003. A nanoindentation study of serrated flow in bulk metallic glasses. Acta Mater. 51 (1), 87–99.
Spaepen, F., 1977. A microscopic mechanism for steady state inhomogeneous flow in metallic glasses. Acta Metall. 25 (4), 407–415.
Spathis, G., Kontou, E., 2001. Mechanism of plastic deformation for polycarbonate under compression by a laser extensometer technique. J. Appl. Polym. Sci. 79 (14), 2534–2542.
Struik, L.C.E., 1977. Physical aging in plastics and other glassy materials. Polym. Eng. Sci. 17 (3), 165–173.
Tanio, N., Nakanishi, T., 2006. Physical aging and refractive index of poly(methyl methacrylate) glass. Polym. J. 38 (8), 814–818.
Voyiadjis, G.Z., Malekmotiei, L., 2016. Variation of the strain rate during CSM nanoindentation of glassy polymers and its implication on indentation size effect. J. Polym. Sci. B Polym. Phys. 54 (21), 2179–2187.
Voyiadjis, G.Z., Samadi-Dooki, A., 2016. Constitutive modeling of large inelastic deformation of amorphous polymers: free volume and shear transformation zone dynamics. J. Appl. Phys. 119 (22), 225104.
Voyiadjis, G.Z., Samadi-Dooki, A., 2018. Hyperelastic modeling of the human brain tissue: effects of no-slip boundary condition and compressibility on the uniaxial deformation. J Mech Behav Biomed Mater 83, 63–78.
Voyiadjis, G.Z., Samadi-Dooki, A., Malekmotiei, L., 2017. Nanoindentation of high performance semicrystalline polymers: a case study on PEEK. Polym. Test. 61, 57–64.
Voyiadjis, G.Z., Malekmotiei, L., Samadi-Dooki, A., 2018. Indentation size effect in amorphous polymers based on shear transformation mediated plasticity. Polymer 137, 72–81.
Voyiadjis, G.Z., Malekmotiei, L., Samadi-Dooki, A., 2019. Continuous stiffness measurement nanoindentation experiments on polymeric glasses: strain rate alteration. In: Voyiadjis, G.Z. (Ed.), Handbook of Nonlocal Continuum Mechanics for Materials and Structures. Springer International Publishing, Cham, pp. 315–332.
Vu, T., Nikaeen, P., Akobi, M., Depan, D., Chirdon, W., 2020. Enhanced nucleation and crystallization in PLA/CNT composites via disperse orange 3 with corresponding improvement in nanomechanical properties. Polym. Adv. Technol. 31 (3), 415–424.
Ward, I.M., 1971. Review: the yield behaviour of polymers. J. Mater. Sci. 6 (11), 1397–1417.
Zhang, G.P., Wang, W., Zhang, B., Tan, J., Liu, C.S., 2005. On rate-dependent serrated flow behavior in amorphous metals during nanoindentation. Scripta Mater. 52 (11), 1147–1151.
Zhang, P., Arceneaux, D.J., Liu, Z., Nikaeen, P., Khattab, A., Li, G., 2018. A crack healable syntactic foam reinforced by 3D printed healing-agent based honeycomb. Compos. B Eng. 151, 25–34.
Zhao, B., Zikry, M.A., 2015. The effects of structural disorders and microstructural mechanisms on semi-crystalline P3HT behavior. Polymer 57, 1–11.